Mehran University Research Journal of Engineering and Technology

https://doi.org/10.22581/muet1982.3281

2024, 43(4) 182-191

Extraction and classification of vibration features of rolling element bearing with increasing the rotational speed

Saima Bhatti [a, *], Asif Ali Shaikh [a], Asif Mansoor [b], Ramsha Shaikh [c]

[a] *Department of Basic Science and Related Studies, Mehran University of Engineering and Technology. Jamshoro 76062, Pakistan*

[b] *Department of Industrial and Manufacturing Engineering, PN Engineering College, National University of Sciences and Technology Karachi 07548, Pakistan*

[c] *Department of Computer Science and Technology, Beijing Institute of Technology, Beijing, 100081, China*

[*] Corresponding author: Saima Bhatti, Email: saima.bhatti@faculty.muet.edu.pk

Received: 04 June 2024, Accepted: 22 September 2024, Published: 01 October 2024

KEYWORDS

Inner Race Faulty Bearing

Outer Race Faulty Bearing

Vibration Analysis

Statistical Features

Kurtogram

Spectral Kurtosis

ABSTRACT

Machinery components degrade over time due to continuous use. A reliable prognosis framework can improve machinery health by monitoring the behavior of its parts and providing warnings before critical failures occur. Bearings, which are essential components of rotating machinery, help maintenance personnel assess the machine's condition during continuous wear. In this study, vibration data from roller bearings under various conditions and faults were collected. The Vibration analysis technique was employed to detect and classify different faults in bearings based on the characteristics of the vibration signals generated by the machinery. Faults can be detected, diagnosed, and classified by analyzing bearing vibration signatures using techniques such as frequency analysis, time-domain analysis, spectral analysis, and kurtogram classifiers. This enables appropriate maintenance actions to be taken in time, preventing further damage or failures.

1. Introduction

In the industrialized era, rotating machines are the backbone of everyday programs and procedures. In the realm of rotating machinery, noise poses a significant challenge for engineers and academic researchers by masking faulty bearing signals, particularly in their initial stages. Early detection and identification of rolling element bearing faults play a crucial role in enhancing the reliability of mechanical components, averting sudden machine failures, and reducing maintenance expenses. In real-world scenarios, defective bearings are responsible for the majority of failures in rotating machinery [2, 3]. The study of bearing faults indicates that from 40% to 90% of failures in both, large and small machines are attributed to damage in rolling element bearings [4]. In general, rolling element bearings are engineered to support axial and/or radial loads while minimizing rotational friction through the placement of rolling elements like cylinders or balls between inner and outer races. They find widespread application across various industries today, serving in production lines, electric motors, pumps, and gearboxes. These bearings may encounter angular, axial, or radial loads depending on the specific design requirements. While ball and roller bearings may seem straightforward, their internal workings are quite intricate. Premature bearing failure can occur under extreme operating conditions characterized by heavy loads, high speeds and very high or low temperatures. Normally the vibration signals of ball bearings in healthy conditions are not smooth, they are essentially generating vibrations. At the existence of a defect, the vibration level is increased in a ball bearing. The nature of defects in a ball bearing such as cracks on the rotating surface, distributed defects, uneven races, etc. The

vibration pattern of these defects is captured by an accelerometer and analyzed using an algorithm. When a rolling element comes across a defect in one of the races, it generates an impulse. As the bearing rotates, these impulses occur periodically at a specific frequency. Modeling is employed to describe the vibration pattern resulting from a single-point defect in the inner race.

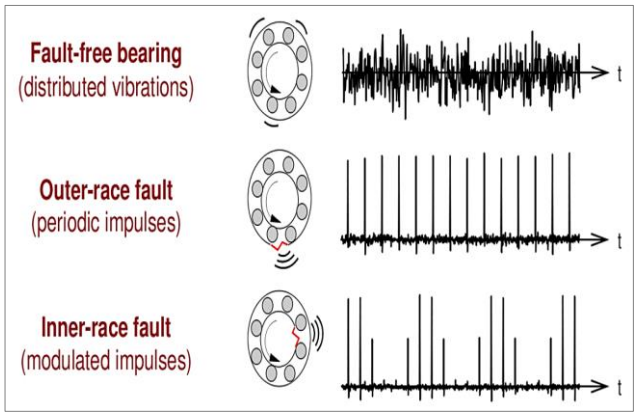

Fig. 1. Possible Defects In Ball Bearing

If a defect emerges on the inner or outer race of the bearing, the frequency at which each rolling element strikes the defect is termed the "Ball-pass frequency," determined by the bearing's geometry and rotation speed. This frequency can be theoretically calculated and compared to the detected frequency post-signal processing, serving as an indicator of the algorithm's efficacy. For more comprehensive diagnosis, such as assessing defect size for decision-making, ball-pass frequencies and a vibration pattern devoid of noise can be valuable. Fig. 1 presents vibration signals from a defect-free bearing and bearings with inner and outer race faults. Notably, the characteristics of impulses stemming from inner and outer race defects differ. Impulses arising from outer race defects exhibit nearly uniform amplitudes, as the race remains stationary relative to the load zone; hence, each rolling element's passage by or strike against the stationary defect on the outer race generates impulses of equal amplitude. In contrast, impulses originating from inner race defects vary in amplitude yet retain periodicity, indicating amplitude modulation. As these impulses stem from resonance within the bearing elements, their amplitude correlates directly with the applied force on the ball bearing. When the inner race of a rotating component, bearing a defect, traverses the load zone—meaning a rolling element encounters the defect as it moves in and out of the load zone—periodic modulated impulses emerge with each shaft rotation. Consequently, the envelope of these impulses can be defined in terms of load distribution.

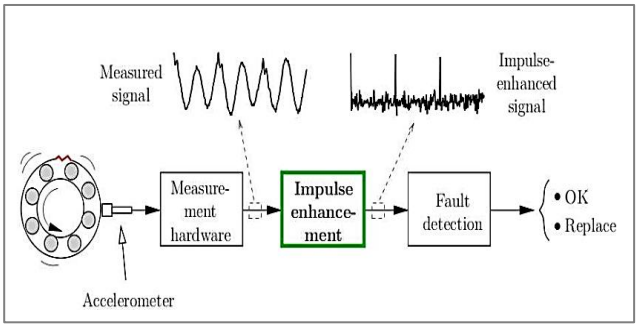

Fig. 2. Fault Detection Process

Following the measurement system, noise, distortions, and disturbances obscure the signals from a faulty bearing. The algorithm aims to restore and amplify these signals by eliminating undesired effects, as depicted in Fig.2. The objective is to accomplish this with minimal computational resources, effort, and complexity, avoiding additional pre-processing steps like filtering or envelope detection, and ensuring the system remains cost-effective.

The vibration analysis is the most common technique used to detect faults in a bearing [5]. The vibrational signals of the fault bearing are non-linear or non-stationary in behaviour due to random noise. The feature extraction process becomes complicated due to this random noise [6].

In the CBM technique to identify the fault in the vibration data of the bearing features extraction approach was applied [7, 8] these features identify the specific pattern related to the fault in the vibration data of the operating machine [9, 10].

The feature extraction technique is also used in predictive maintenance methodology [11]. The extracted features are further used in the predictive models to forecast the health of a machine [12]. The forecaster's result helps to make decisions about the condition of an operating machine [13, 14].

2. Experimental Setup

The test rig is shown in Fig: 3 in which an induction motor is attached to a central shaft supported by two bearings. A UC-203 deep groove ball bearing is attached to the central shift.

Fig. 3. Experimental Setup

In which one end of the shaft is placed on a healthy bearing, whereas the other end is used for testing different faulty bearings. The motor running speed ranges from 0-3000 rpm. The vibration analyzer CSI IEPE is utilized for quantifying the performance of the varying faulty bearings. It has a sensitivity of 5.01 mV/g with a frequency range of 1 to 12 kHz and a measuring range of up to ± 500g. The real-time data was collected by utilizing NI DAQ. The arrangement of the experimental setup is shown in the Fig 3. The parameters of the understudy bearing are presented in Table 1.

Table 1

The bearing specification

Specification	UC-203
Bore diameter (d mm)	17
Outside diameter (D_{SP} mm)	47
Width (B mm)	31
Width outer ring (C mm)	17
Sealing total width (C_2 mm)	16.8
Distance raceway (S mm)	12.7
Width of flats (W mm)	3
Rib diameter inner ring (d_1 mm)	27.56
Number of the balls	8
Contact angle (degree)	0^o

Besides, three bearing conditions were examined: normal bearing, bearing with inner and outer race fault. Primarily, baseline data were obtained using normal bearing experiments. Secondly, data with inner and outer race faults were collected. Vibrant data for inner race, outer race faulty, and healthy bearing is sampled at 200000 Hz for the duration of 10 seconds.

3. Methodology

Vibration analysis is a crucial tool in the fields of monitoring and classification of the health of rotating machinery. Extracting features from vibration data is essential for understanding the behaviour of the system under study and for predictive maintenance purposes. The methodology to analyze the behaviour of fault in the bearing, the vibration analysis technique, required the following steps:

3.1 Collection of Data

From the experimental setup, sensors such as the accelerometer were used to collect the real-time vibration data of healthy bearings and faulty bearings. To capture the data at regular intervals over a specific period to understand the dynamical behavior of the bearings.

3.2 Processing of Data:

The data processing is the second step of this methodology which transforms the baseline data into tangible characteristics of the signal data. For this purpose, the FFT technique is used to convert a time-domain signal into a frequency-domain signal.

$$\text{FFT}= \sum_{i=1}^{n} x_i(t) \exp(i\, 2\pi\, k/n) \qquad \text{Eq. (1)}$$

Where $x_i(t)$ represents the time domain vibration signal and k represents the period signal. After converting the time-domain signal into the frequency domain, the power spectrum is used to estimate the distribution of power across the frequency range.

$$\text{Power spectrum= sqrt } |\text{FFT}| \qquad \text{Eq. (2)}$$

To detect the fault in the frequencies the envelope spectrum is used in this framework.

$$\text{Envelop spectrum}=x(t) + iy(t) \qquad \text{Eq. (3)}$$

Where $x_i(t)$ represents the time domain vibration signal $y(t) = \frac{1}{\pi}\int_{-\infty}^{\infty} \frac{x(\tau)}{x(t-\tau)} d\tau$ Hilbert Transform.

3.3 Feature Extraction

After processing the experimental data into significant statistics the third step of the methodology is feature extraction. The feature extract is a technique to obtain the significant characteristics of the signal data. These observing signals have many details of health state and measurement noise. Features are classified using RMS, kurtosis, skewness, Crest Factors, peak value, Visual, particle count, spectrograph, etc. In this study, we extracted the features of the recorded data in the time domain and frequency domain under the increasing rotating speed of the machine.

The statistical quantification of bearing data was extracted we proposed the statistical vibration acceleration moments of a distribution signal because it can be used to measure the statistical features. The moment coefficients of time signal data can be calculated using Eq(4).

$$Mn = E[X^n] = \frac{1}{N}\sum_{i=1}^{n}(x_i(t))^n \qquad \text{Eq. (4)}$$

where $E\{X^n\}$ represents the expected value of the function, x_i is the timehistorical data and N is the number of data points. The first four cumulates: mean, standard deviation, skewness, and kurtosis, can be calculated from the first four moments using the following relationships.

$$Mean = M_1 \qquad \text{Eq. (5)}$$

$$Standard\ Deviation\ = M_2 \quad \text{Eq. (6)}$$

$$Skewness = M_3 - 3M_2M_1 + 2M_1^3 \quad \text{Eq. (7)}$$

$$Kurtosis\ = M_4 - 3M_2^3 - 4M_3M_1 + 12M_2M_1^2 - 6M_1^4 \quad \text{Eq. (8)}$$

3.4 Classification Model

The non-stationary behavior in the frequency domain and also their locations in the frequency domain. The spectral kurtosis (SK) of a signal $x(t)$ can be calculated using the short-time Fourier transformation (STFT) of the signal [15].

$$S(t,f) = \int_{-\infty}^{\infty} \boldsymbol{x_i(t)} w(t-\tau) e^{-2\pi f t} dt \quad \text{Eq. (9)}$$

Where $w(t)$ is the window.

$K_{\boldsymbol{x_i(t)}}(f) = \frac{\langle |S(t_i,f)|^4 \rangle}{\langle |S(t_i,f)|^2 \rangle^2} - 2, \quad f \neq 0$ and $\langle . \rangle$ is the mean operator in time.

A kurtogram classifier for bearing fault detection involves using the kurtogram method to analyze vibration signals from bearings and classify them based on fault conditions.

3.5 Fault Diagnosis

This involves determining the specific type and severity of the fault, based on the features extracted from the vibration data and the results of the fault detection process. This information can be used to develop a maintenance plan and to prioritize repairs.

4. Results and Discussion

The dissimilarity in trend is classified into three classes concerning healthy and unhealthy bearing, with inner and outer race faults. Primarily, the vibration spectrum for healthy bearings is analyzed, which exhibits a smooth pattern. Subsequently, the observed spectrum lowered then stabilized or fluctuated in between due to damage promulgation during experimentation.

a) Healthy Bearing Features with Increasing Speed

The process of vibration analysis starts with applying the algorithm on a perfectly working and healthy bearing undergoing regular increases in rotational speed. The healthy bearing time domain data collected for a duration of 10 seconds is plotted in Fig 4, which shows the double amplitude from the starting amplitude as evident from the rotating speed, which varies from 14.1 Hz to 23.8 Hz

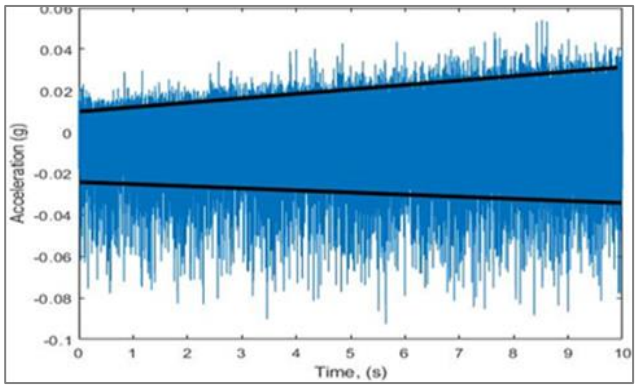

Fig. 4. Healthy Bearing Increasing Speed Time-Domain Plot

Fig.5 is a zoomed plot to 100X in the time domain between 0 to 0.1 seconds, which signifies the smoothness in the vibrant data. The spikes generated during this plot are because of the increase in rotational speed at each cycle.

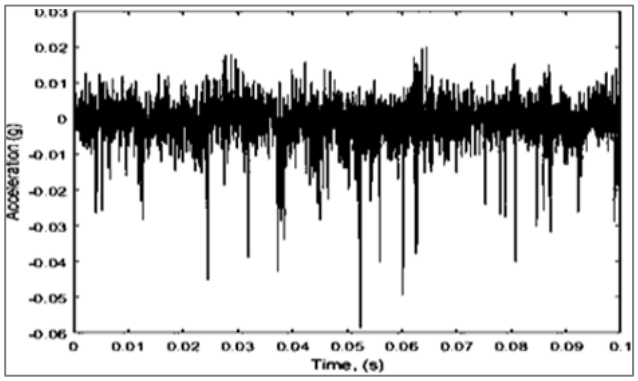

Fig. 5. Zoomed In View Of Time-Domain Plot

To cater to these spikes, we converted the data into the frequency domain by utilizing the Fast Fourier Transform (FFT).

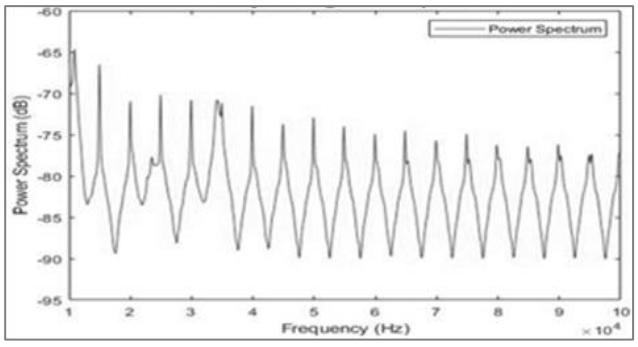

Fig. 6. Zoomed Given Time-Domain Plot

The power spectrum acquired by converting data into the frequency domain is displayed in Fig 6, which shows that the frequency domain plot is regular and smooth, which authenticates the healthy behavior of the bearing during the functioning of the motor. The Eq. obtained by utilizing frequency data is as follows:

$$f(x) = -80.36 + 4.59\ Cos\ wx + 0.66\ Sin\ wx \quad \text{Eq. (10)}$$

To cross-validate the results, the computed and observed frequency is plotted as shown in Fig 7, which

signifies the power of the estimate of the frequency for healthy bearing.

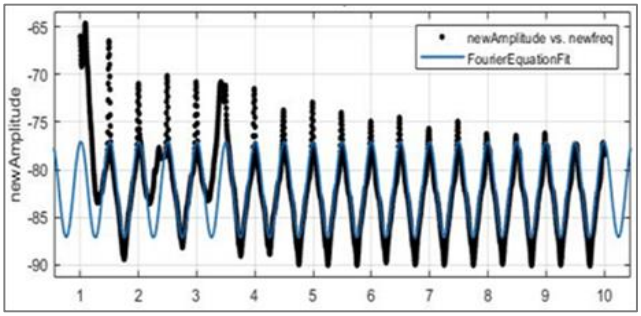

Fig. 7. Computed And Estimated Frequency Plot

Now, the envelope spectrum analysis is performed to bifurcate the unwanted signal from the desired signals. These unwanted signals might be accumulated from machinery operating conditions or any other specific noise.

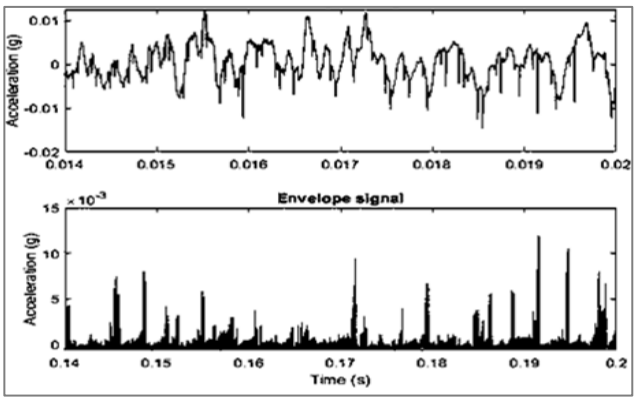

Fig. 8. Healthy Bearing Envelope Spectrum Analysis

The outcomes of the envelope spectrum are divided into two groups as displayed in Fig 8, in which the upper portion represents the signal received from the data, whereas the lower part characterizes the signal after envelope spectrum analysis.

The signal in the lower portion indicates the unwanted signals in the data set whose zoomed-in view is represented in Fig 9, which is considered to monitor harmonics in the whole process. The above graph does not display any particular impulse for ball pass frequency outer (BPFO) or ball pass frequency inner (BPFI). Therefore, it confirms the health of the bearing during machinery operation.

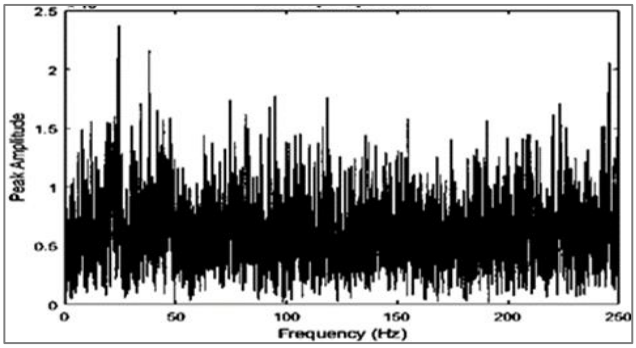

Fig. 9. Zoomed-In View To Monitor Harmonics

b) Inner race faults Bearing Features with increasing the rotational speed

In this case, bearing data with inner race faults for increasing speed is considered. The behavior of the data in the time domain is displayed in Fig 10.

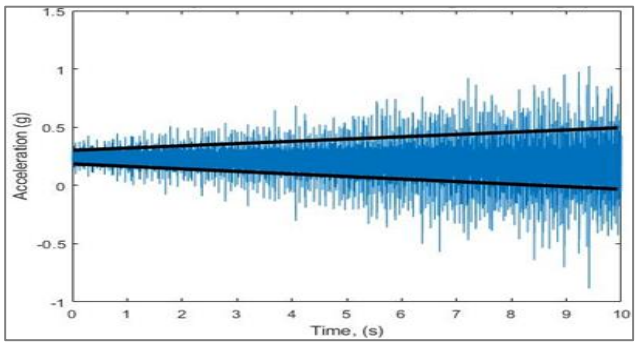

Fig. 10. Time Domain Behaviour Of Inner Race Faulty Bearing

The plot indicates irregularities and abnormal growth in amplitude concerning time amplifications. These enormous deviations in amplitude certified the inadvertent impulsiveness in the bearing. It has also been noticed that rotation speed accelerated from 12.5Hz to 27.5Hz, increasing its amplitude to two-fold, and generating an error of three hundred percent.

The zoomed-in view portrayed in Fig 11 displays considerable variations every 0.03 seconds, which indicates the inner race fault after the completion of a complete revolution.

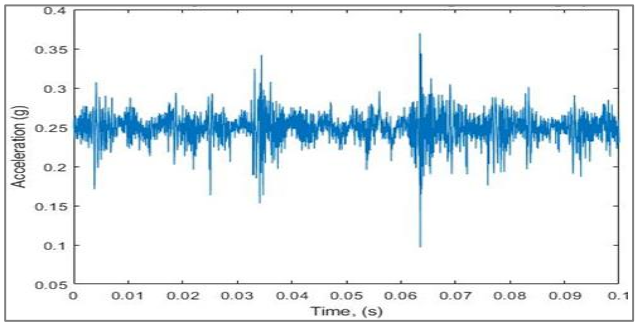

Fig. 11. Time Amplitude Variation Of Inner Race Fault

To look into the in-depth variation in the waveform Fourier transform is implemented as illustrated in Fig 12.

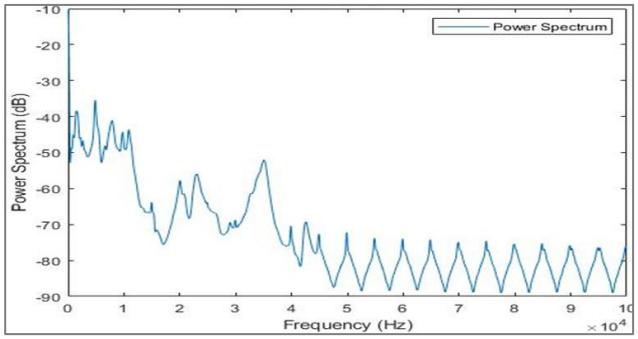

Fig. 12. Frequency Power Spectrum Plot For Inner Race Fault

The power spectrum exhibits robust disorder in the preliminary portion, which indicates undesired frequencies initiated by the inner race fault in the bearing.

The estimated Fourier transform Eq. is as follows:

$$F(\omega) = 5.328 + \sum_{i=1}^{i=8} A_i \, Cos(\alpha_i \omega) + \sum_{j=1}^{j=8} B_j \, Cos(\beta_j \omega)$$

Eq. (11)

where $F(\omega)$= Fourier Transform function of vibration amplitude

$A_1\,(for\ \alpha_1 = 1) = 127.93\,,\ A_2\,(for\ \alpha_2 = 2) = 29.61$

$A_3\,(for\ \alpha_3 = 3) = -47.89,\ A_4\,(for\ \alpha_4 = 4) = -73.78$

$A_5\,(for\ \alpha_5 = 5) = -53.54,\ A_6\,(for\ \alpha_6 = 6) = -19.91$

$A_7\,(for\ \alpha_7 = 7) = 1.01,\quad A_8\,(for\ \alpha_8 = 8) = 3.75$

$B_1\,(for\ \beta_1 = 1) = -87.75, B_2\,(for\ \beta_2 = 2) = -128.9$

$B_3(for\ \beta_3 = 3) = -98.67,\ \ B_4\,(for\ \beta_4 = 4) = -31.28$

$B_5\,(for\ \beta_5 = 5) = 18.32,\quad B_6\,(for\ \beta_6 = 6) = 29.69,$

$B_7\,(for\ \beta_7 = 5) = 18.77,\quad B_8(for\ \beta_8 = 5) = 6.45$

Eq (11) indicates various harmonics that specify that the bearing is running with numerous impulses or unbalanced forces that were not observed in the running of a healthy bearing.

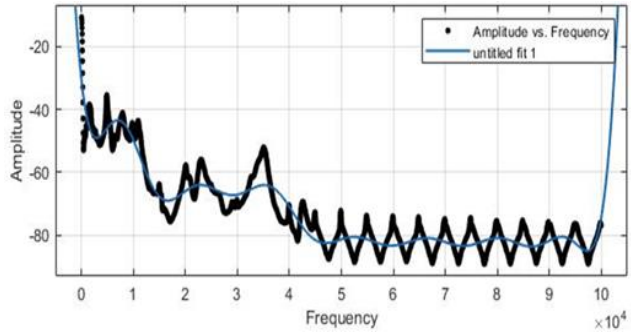

Fig. 13. Computed Versus Observed Plot

In order to quantify the fault by utilizing the data pattern, the technique of envelop spectrum analysis is implemented.

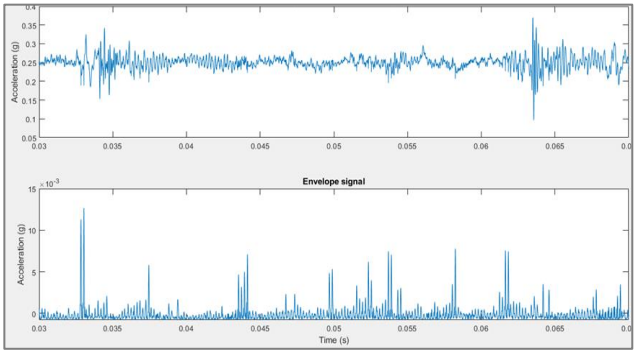

Fig. 14. Noisy (Upper) And Non-Noisy (Lower) Envelope Spectrum

The outcomes of the envelope spectrum are divided into two groups as displayed in Fig 14, the upper portion displays the observed signal that includes noise and surplus disturbance on the floor, while the lower portion displays the resulting waveform after the envelope spectrum analysis. These resulting waveforms indicate considerable spikes and irregularities as evident from the lower portion of the graph.

These resulting waveforms indicate considerable spikes and irregularities as evident from the lower portion of the graph. Fig:15 represents harmonics at the BPFI.

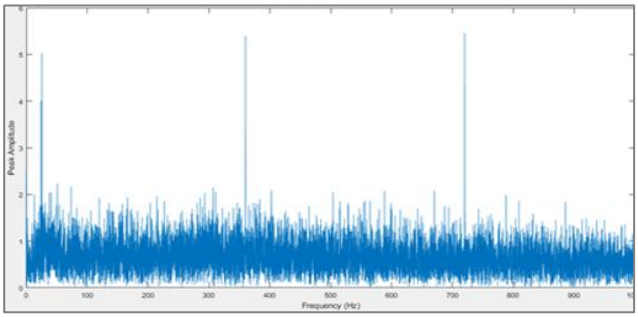

Fig. 15. Significant Harmonics For Inner Race Fault

These frequencies are vital parameters to identify any defects in the inner race of the bearing. As we can see, a significant peak at these frequencies confirms the presence of unbalanced forces or impulses at these points. This analysis is adequate in deciding the bearing dataset and in identifying faults in the bearing.

The comparison of kurtosis for healthy and unhealthy bearing is illustrated in Fig:16.

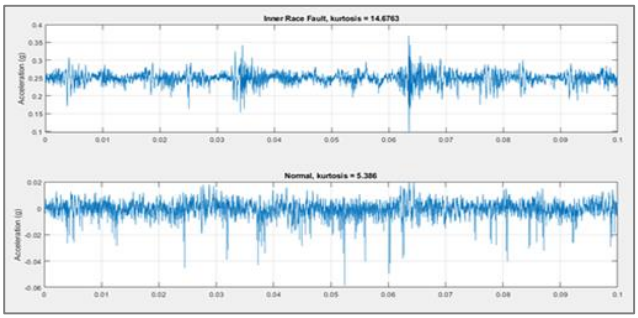

Fig. 16. Comparison Of Kurtosis With Healthy V/S Unhealthy Bearing

The diagram is separated into two parts, with the upper part displaying the signal from the faulty bearing having a kurtosis value of almost 15. Besides, the lower part displays the healthy bearing signal having a kurtosis value of 5.

This means that a bearing with a defect in the inner race fault would usually have a kurtosis value difference of three-fold more than a healthy bearing. In such cases, it can be significantly deduced that the bearing has an inner race fault.

c) Outer race faults Bearing Features with increasing the rotational speed

Now, we quantify the behaviour in the signal observed for bearings having outer race faults with increasing speed. The time domain variation in the signals for such faults is represented in Fig 17. The above Fig. shows the growths in the amplitude and is estimated that it generates a fifteen percent error in amplitude progression from start to end between theoretical and actual values.

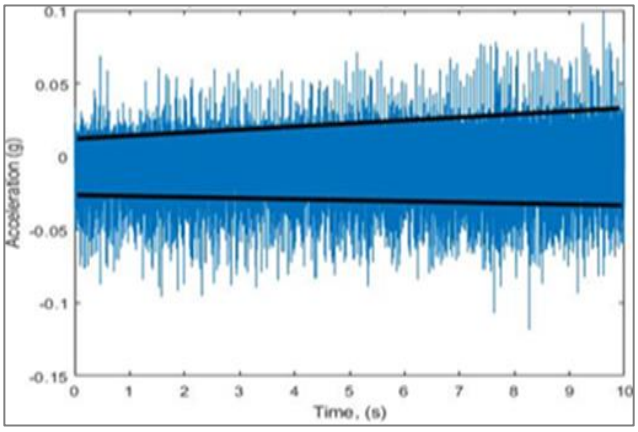

Fig. 17. Time Domain Variation In Outer Race Faulty Bearing, Increasing Speed

It has been observed that the bearing dataset of the inner race fault has a much higher level of impulsiveness than the bearing of the outer race fault. In contrast, the proportion of the increase is the same as the lower error percentage. The plotting zoomed-in view in Fig 18 does not enable us to detect faults in the bearing.

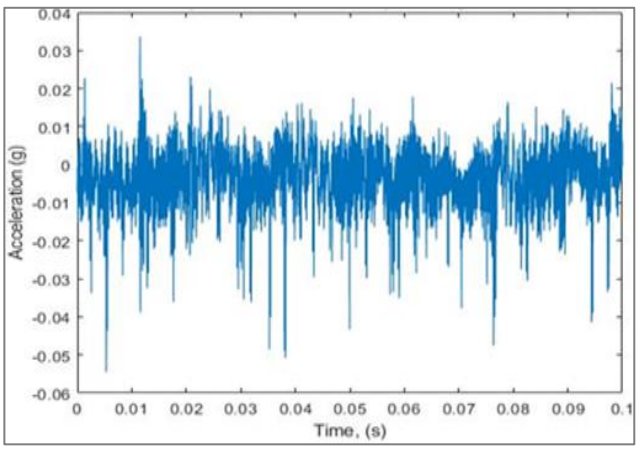

Fig. 18. Zoomed-In View Of Outer Race Faulty Bearing

The Fourier transform estimation of the entire signal is adopted to identify unwanted or faulty frequencies in the outer race defective bearing data whose plot is underneath Fig:19.

The result of the Fourier Transform (FT) impulsiveness for an outer race faulty bearing falls in between healthy and an inner race faulty bearing impulsiveness.

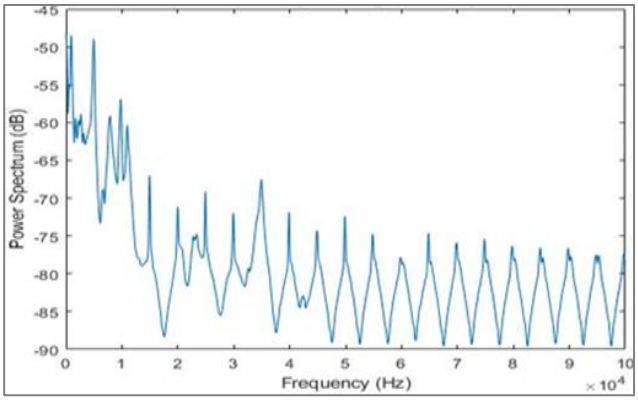

Fig. 19. Fourier Transform Data Of Outer Race Faulty Bearing

The Fourier transform estimated Eq. yields as follows:

$$F(\omega) = -77.54 + \sum_{i=1}^{i=4} A_i \, Cos(\alpha_i \omega) + \sum_{j=1}^{j=4} B_j \, Cos(\beta_j \omega)$$

Eq. (12)

$A_1(for\ \alpha_1 = 1) = 8.96\ , A_2(for\ \alpha_2 = 2) = 4.95$

$A_3\ (for\ \alpha_3 = 3) = 3.69, A_4\ (for\ \alpha_4 = 4) = 1.721$

$B_1\ (for\ \beta_1 = 1) = 0.18, B_2\ (for\ \beta_2 = 2) = -1.11$

$\mathrm{B_3\ (for\ \beta_3 = 3) = -1.59, B_4(for\ \beta_4 = 4) = -0.57}$

Eq (12) indicates that although the signal does contain harmonics and unwanted frequencies, they are not as much as the ones included in the inner race-bearing fault. The outer race fault bearing right in the centre of a healthy bearing and with one a fault in the inner race.

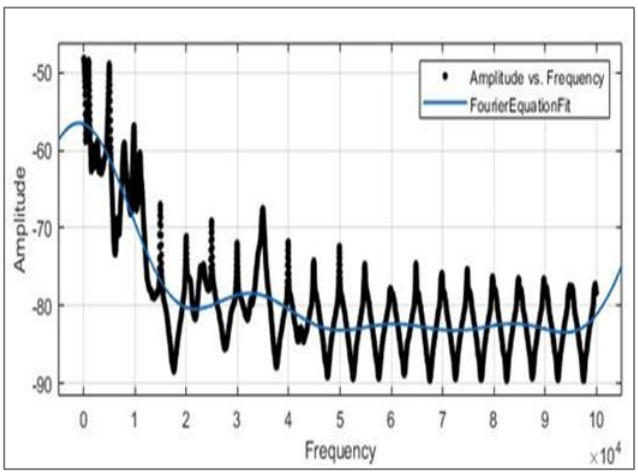

Fig. 20. Fourier Fit On Fourier Transforms

To quantify the fault by utilizing the data pattern, the technique of envelop spectrum analysis is implemented. The computed result of the envelope spectrum is presented in Fig:21, which confirms the elimination of floor noise and unwanted signals. These signals were now further studied for the identification of faults.

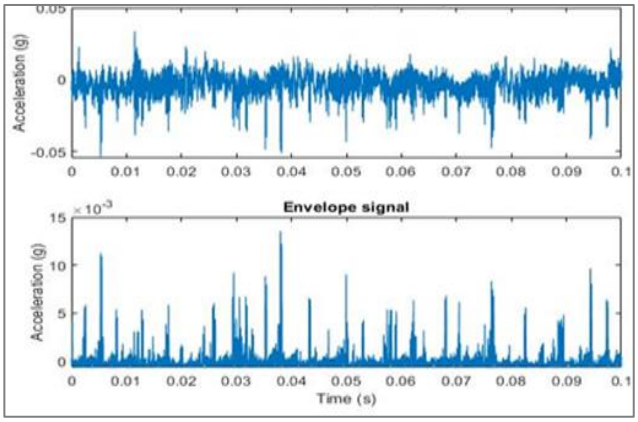

Fig. 21. Envelope Spectrum Of Outer Race Faulty Bearing

The Fourier transform of the envelope is plotted in Fig:22 to signify the peaks generated by the faulty bearing signals during the increasing speed of the understudy system.

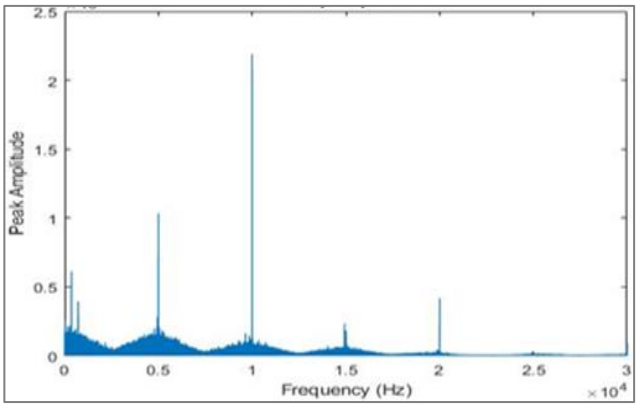

Fig. 22. Targeted View For Indicating Harmonics

These harmonics are adjacent to the faulty frequencies observed in the inner race defective bearing. To quantify the exact fault of the bearing, an analysis of the kurtosis is performed for vibration signals. The kurtosis plot is presented in Fig:23 with an estimated value of 5.981.

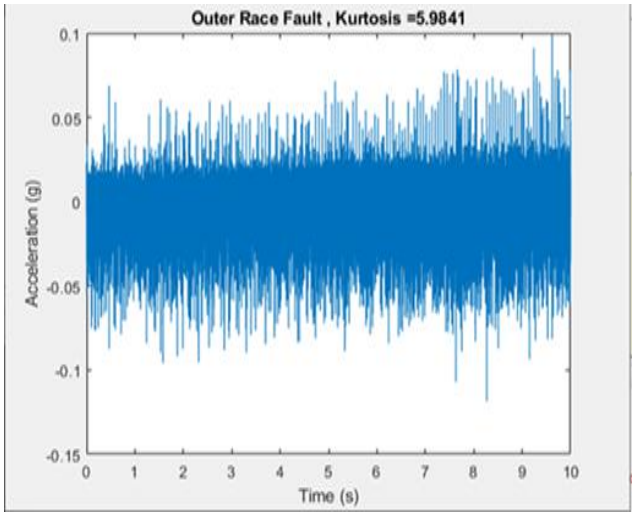

Fig. 23. Estimated Kurtosis Plot For Outer Defective Bearing

Table 2 presents the significant statistics of the healthy bearing, inner race faulty bearing, and outer race faulty bearing data. The kurtosis values of inner race faulty bearing are very high (approximately 15) which indicates that inner race fault.

Table 2

Important statistics for the Healthy, Inner race & Outer race Faulty bearing data set

Statistical Features	Healthy bearing	Inner race Faulty bearing	Outer race Faulty bearing
Mean Value	5.22e-04	0.2069	0.0016
Root Mean Square	0.0072	0.2133	0.0098
Standard Deviation	0.0071	0.0520	0.0097
Kurtosis	5.38	14.6763	5.98

It has been noticed that the amount of deviation of the faulty bearing is not sufficient to quantify the defect of the outer race faulty bearing. In pursuance of the defect caused by the outer race faulty bearing, further analysis is performed by utilizing the techniques of kurtogram and spectral kurtosis.

Lastly, a kurtosis value was computed for cross-validation of the impulsiveness of the vibration signal for increasing speed. The estimated spectral kurtosis value for the understudied case was observed to be 5.38, which is neither maximum nor minimum. Consequently, the dataset for the concerned bearing is classified as healthy.

The program of the corresponding signal is specified in Fig:24, which categorizes key parameters of the signal including its bandwidth and maximum kurtosis value at a certain point. The bandwidth of the signal is detected at 50kHz with a central frequency of 75kHz. The kurtosis value in the bandwidth 50kHz indicate the irregularities in the vibration signal or fault.

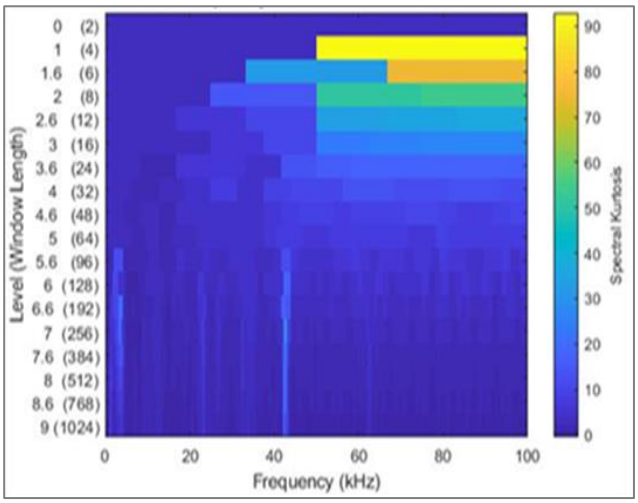

Fig. 24. Kurtogram Of Outer Race Faulty Bearing

By employing statistics specified in the program, a spectral kurtosis is performed to identify unwanted frequencies in the signal for quantifying faults in the outer race of the bearing.

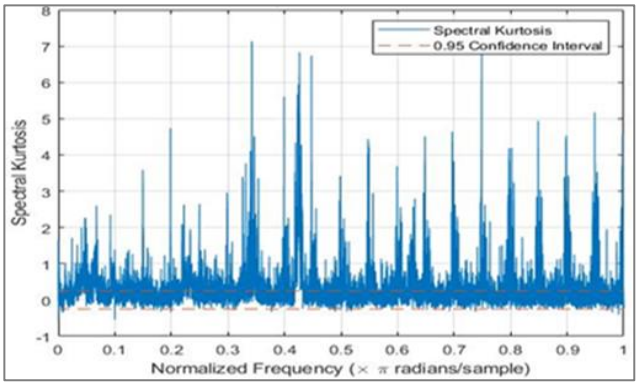

Fig. 25. Spectral Kurtosis Of Outer Race Faulty Bearing

The result of the spectral kurtosis is presented in Fig:25 which represents the peaks that are unwanted or induced due to the fault in the bearing. Since the faulty bearing applied forces are not balanced it produces numerous impulses of countless frequencies as illustrated in Fig:25. It precisely quantifies the fault induced by the outer race defective bearing.

5. Conclusion

In this study behaviour of healthy, inner race, and outer race faulty bearing with increasing speed was quantified by utilizing vibration techniques. This study reveals that signals of healthy bearing are regular and smooth. Besides estimated Eq. perfectly follows the observed data. In the second case, the behaviour of the vibrational signal is increased without any bounded, due to unwanted harmonics, and irregularities. The impulses are being repeated at the BPFI (Ball Pass Frequency Inner) which indicates the bearing inner race fault. The estimated kurtosis for this case is around 15 which specifies the fault in the bearing. In the third case, it can be observed that the waveform is highly irregular, contains unwanted frequencies, and has multiple spikes. The kurtosis value of 5.98 does not quantify outer race fault at this stage. In this case, the fault is quantified by utilizing the spectral kurtosis technique that Identifies the frequency range where outer race fault transients occur. Isolates BPFO and other fault-specific frequency bands affected by the outer race fault, and provides greater diagnostic.

6. References

[1] M.N. Albezzawy, M.G.A. Nassef, E.S. Elsayed, A. Elkhatib. "Early Rolling Bearing Fault Detection Using a Gini Index Guided Adaptive Morlet Wavelet Filter", 10th IEEE conference, p.314-322, 2019.

[2] M.Hussain,A.Mansoor, Rehman, S.Nisar, " Bearing degradation prognosis using structural brak classifier", Mechanika vol,24 no.4,p.456-461,2018 https://doi.org/10.5755/j01.mech.4.24.20740

[3] M.Hussain, A. Mansoor,A. Rehman, "A novel approach for machinery health prognostics using statistical tools", *Proceedings of 50th MFPT Conference 2017,* pp. 1–13,2017

[4] X.Liu, L.Bo, X.He, M.Veidt, "Application of correlation matching for automatic bearing fault diagnosis", J. Sound Vib.vol. 331, p.5838–52 ,2012

[5] W.Li, M.Qiu, Z. Zhu, B.Wu, G.Zhou, "Bearing fault diagnosis based on spectrum images of vibration signals", Meas. Sci. Technol. Vol.27 ,p.035005, 2016

[6] C. Bianchini, F. Immovilli, M. Cocconcelli, R. Rubini, and A. Bellini, "Fault detection of linear bearings in brushless ac linear motors by vibration analysis", IEEE Transactions on Industrial Electronics, vol. 58, no. 5, pp. 1684–1694, May 2011

[7] L.Xu, Z.Gao ,J.Pan, "Rolling bearing fault diagnosis under variable conditions based on intrinsic time-scale decomposition and optimized support vector machine", Measurement, vol.73, p.142-154, 2015

[8] C.L.T Borges, Alves, M. A., J.A Dente, "A review of feature extraction methods for gearbox fault diagnosis based on vibration signals", Mechanical Systems and Signal Processing, vol.145, p.106953,2020

[9] X.Jiang, Y.Cai, X.Ding, "Feature extraction methods for fault diagnosis of rolling element bearings: A review", Mechanical Systems and Signal Processing, vol.146, p.107045,2020.

[10] Kang, J., & Wang, Z. "An adaptive neuro-fuzzy inference system for tool wear monitoring using wavelet features", Measurement, Vol.80, p.127-135, 2016.

[11] Wang, D., Zhang, X.,Li, W. "Feature extraction and fault diagnosis of rolling bearings using combined convolutional denoising auto encoder and deep belief network". IEEE vol.7, p.109687-109700.2019

[12] B.Xia, L.Zhang,Z.Feng "Feature extraction and selection for mechanical fault diagnosis: A review", IEEE Access, 9, p.15077-15093, 2021

[13] S. Bhatti, A. Shaikh, A. Mansoor, “A Investigation the fault in a Rotating Machine by Utilizing Vibration Technique”, SURJ.vol.54 No.2 2022

[14] S. Bhatti, A.A. Shaikh, A.Mansoor, M. Hussain, “New Approaches of Stochastic Models to Examine the Vibration Features in Roller Bearings”, Appl. Sci.,vol.14 ,no.4 ,2024 https://doi.org/10.3390/app14041616

[15] J. Antoni, “The spectral kurtosis: a useful tool for characterising non-stationary signals”, Mechanical Systems and Signal Processing, vol. 20, no. 2, pp. 282–307, Feb. 2006, dio: 10.1016/j.ymssp.2004.09.001

